Rotating Electroosmotic Flow of Viscoplastic Material Between Two Parallel Plates

Cheng Qi, Chiu-On Ng[1]

Department of Mechanical Engineering, The University of Hong Kong, Pokfulam Road, Hong Kong

Abstract

This study aims to investigate electroosmotic flow of a viscoplastic material, modeled as either Bingham plastic or Casson fluid, through a parallel-plate channel that rotates about an axis perpendicular to the plates. A relatively small yield stress, comparable to that of human blood, is considered in order to confine to the condition there is only one yield surface in the flow. An iterative finite-difference numerical scheme is developed to solve the Cauchy momentum equations and nonlinear constitutive equations. The location of the yield surface, and velocity and stress components in both the sheared and unsheared regions are found as functions of the yield stress, rotation speed and Debye parameter. Numerical results are presented to reveal that the system rotation and yield stress may counteract each other in controlling the resultant flow rate and flow direction. The effect of yield stress may even be reversed for a sufficiently large rotation speed.

Keywords: electroosmotic flow; electric double layer; viscoplastic yield stress; system rotation.

[1]Corresponding author. Tel: (852) 2859 2622; Fax: (852) 2858 5415; E-mail address: cong@hku.hk (C.-O. Ng).

1 Introduction

Electroosmotic pumping is one of the commonly used mechanisms to drive fluid flow in microfluidic applications [1]. The so-called electroosmotic (EO) flow is induced when free charges that are formed in an electrolyte solution near a charged solid surface are set into motion under the action of an applied electric field [2]. Because of the two-layer structure of the ion distribution, a near-wall layer with unbalanced charges is called an electric double layer (EDL). Outside this layer, the solution is essentially electrically neutral. Being charged, fluid in the EDL will be driven into motion by the electric body force when an electric field is applied externally. Through viscous action, fluid outside the EDL will be dragged into motion as well. Compared with pressure-driven flow, EO flow has the advantage that, for sufficiently thin EDLs, the flow-rate is less restricted by the geometric dimension of confinement, and EO pumping is therefore a more suitable mechanism for transporting fluid through very narrow channels.

The increasing need to understand the behaviors of complex fluids (e.g., blood, DNA solutions, colloidal and cell suspensions) in microfluidic analysis has spurred many researchers to study EO flow of non-Newtonian fluids through microchannels in recent years. These studies include, among others, Das and Chakraborty [3], Zimmerman *et al.* [4], Zhao *et al.* [5], Olivares *et al.* [6], Zhao and Yang [7, 8], Babaie *et al.* [9], Vakili *et al.* [10], Ng [11], Ng and Qi [12, 13], Dhar *et al.* [14], Zhu *et al.* [15], and Qi and Ng [16, 17]. A variety of models, such as power-law, Carreau and viscoplastic models, have been used by these authors to describe the non-Newtonian rheology of the material under investigation.

An emerging technique in microfluidics is to mount a system on a fast spinning compact disc (CD), thereby known as CD-based fluidics. The liquids therein are driven by the centrifugal force arising from the system rotation. Centrifugal microfluidics is seen to be a promising tool for high-efficiency flow control and mass separation. Centrifugation is a more appropriate mechanism for transporting fluid with trapped bubbles or gas, and for the equality of mixing fluids. Other advantages like portability, low-cost fabrication, ease of miniaturization and multiplexing, as well as a wide range of attainable fluid pressure

and flow rates are also the merits of centrifugal microfluidics [18, 19].

To capitalize on the advantages of centrifugal and electric forces, Wang *et al.* [20] proposed a CD-like electrophoresis-based biomedical separation system. Their experimental results showed that prolonged electrophoretic separation time and shortened length of channels could be achieved by applying the two forces in opposite directions. Their system was reported to have other advantages like low joule-heat generation, low chemistry reaction and steady ion concentration during the process [20]. The first theoretical study on EO flow in a rotating frame is due to Chang and Wang [21], who derived analytical solutions for rotating EO flow in two geometries (over a single plate and between two parallel plates). Motivated by the work of Chang and Wang [21], Ng and Qi [22] examined the problem for EO flow in a rotating rectangular microchannel. Analytical solutions for the velocities of the primary and secondary flows as well as the induced pressure as functions of electrokinetic and rotation parameters were obtained by these authors using the method of eigenfunction expansion. More recently, Gheshlaghi *et al.* [23] developed closed-form solutions for transient EO flow in a rotating channel, while Shit *et al.* [24] numerically investigated the effect of wall slip on EO flow through a rotating parallel-plate microchannel with a slowly varying cross-section.

As explained above, non-Newtonian models have to be used to describe the complex rheological behaviors exhibited by biological liquids or polymeric suspensions. This has motivated several studies on EO flow of non-Newtonian fluid in a rotating environment. Xie and Jian [25] extended the problem of Chang and Wang [21] to rotating EO flow of power-law fluids between two parallel flat plates. They conducted a parametric study to look into effects of the flow behavior index, rotation speed and zeta potential on the classical EO flow profile. More recently, Li *et al.* [26] and Abhimanyu *et al.* [27] presented numerical models for rotating EO flows of third-grade and viscoelastic fluids, respectively.

The present study aims to investigate EO flow of a viscoplastic material under the effect of system rotation. A viscoplastic material is characterized by the presence of a yield stress in its constitutive relationship between stress and shear rate. The material is not sheared until the stress is higher in magnitude than the yield stress. To determine the motion of a viscoplastic material is in general a challenging problem because it needs to

locate, as part of the solution, the yield surface that separates the flow into sheared and unsheared regions, where different constitutive equations will apply. Hence, unless the problem can simplify to a one-dimensional simple shear problem, the flow of a yield-stress material is a strongly nonlinear problem that has to be solved numerically, typically by means of an iterative scheme.

Viscoplastic models are often used to describe the rheology of blood [28,29]. The magnitude of yield stress in human blood is typically on the order of 5 mPa (or 0.05 dyne/cm^2) at room temperature [30–34]. Such a small value of yield stress is often thought to be physiologically insignificant for blood flow in large vessels. However, in EO flow even a small yield stress can result in appreciable effect. As is known, a pure EO flow has a plug-like velocity profile: the velocity grows sharply in the near-wall EDL region and is uniform (called the Helmholtz–Smoluchowski velocity) in the core. For Casson fluid, Ng [11] found that the presence of even a small yield stress can materially lower the Helmholtz–Smoluchowski velocity. Ng and Qi [12] further examined various effects of the yield stress of three kinds of viscoplastic materials, namely Casson, Herschel–Bulkley and Bingham plastic, on EO flow in a non-rotating slit channel with walls of arbitrary zeta potential. Based on these previous studies, it is the intention of the present work to find out how the yield stress of two particular kinds of viscoplastic materials, viz. Bingham plastic and Casson fluid, may influence EO flow in a rotating slit channel.

The problems considered by Ng [11] and Ng and Qi [12], for EO flow in a non-rotating channel, involve only simple shear flows, and hence the stress distribution can be determined prior to finding the velocity. Consequently, the location of the yield surface, where the stress equals the yield stress, can also be determined in advance. This facilitates the division of the flow into sheared (or yielded) and unsheared (or unyielded) regions, and the velocity can then be found straightforwardly by integrating the stress–shear rate relationship. The problem becomes more complicated when the flow is subject to system rotation. In addition to the primary flow along the axial direction, there is also secondary flow induced by the Coriolis force in the transverse direction. The problem formulation consists of multi-dimensional Cauchy momentum equations and nonlinear constitutive equations, with velocity and stress components being the variables. The

location of the yield stress is also an unknown that has to be found simultaneously with the other unknowns (velocity and stress components). Solving for these unknowns can therefore be a very onerous process.

One objective of the present work is to devise an iterative numerical scheme to solve for the unknowns (including the location the yield stress, velocity and stress components) in the problem of EO flow of Bingham plastic and Casson fluid in a rotating slit channel. To circumvent the difficulty arising from the yield stress, many researchers have adopted the so-called regularization method to approximate the sheared/unsheared constitutive equations by a modified smooth constitutive equation that works everywhere in the flow field without the need to distinguish between sheared and unsheared regions. Some notable modified constitutive equations for Bingham plastic have been proposed by Papanastasiou [35], Bercovier and Engelman [36], and Allouche *et al.* [37]. A regularization scheme is essentially to replace a viscoplastic model, of which the viscosity is finite/infinite in the sheared/unsheared regions and hence a non-smooth function of the shear rate, by a modified model with an effective viscosity that is a smooth function of the shear rate. Through a numerical regularization parameter, the effective viscosity can be adjusted to change sharply with a small departure of the shear rate from zero, like a true viscoplastic material, but in a smooth manner. An advantage of the regularization method is that, in the process of finding solution, the differentiation between sheared and unsheared regions is not necessary. This convenience, however, brings forth a drawback: the position of the yield surface cannot be accurately determined using this method, especially when the yield stress is small. Furthermore, despite the smoothness, the sharp change of the effective viscosity at small shear rates can cause slow convergence, or even divergence, when numerically solving the equations. In this study, the regularization method is not used, and we shall use the original two-region constitutive equations to model Bingham plastic and Casson fluid in our problems. This will facilitate us to find out how the yield stress may modify the flow under the effect of system rotation. A small yield stress comparable to that of human blood is considered. We shall show that even a small yield stress may lead to appreciable effect in rotating EO flow.

It is also for a technical reason that we should limit the yield stress to a certain

value. This is because a rotation of high speed may result in a non-monotonic stress distribution. Therefore, there is a single yield surface only when the yield stress is not too large. Otherwise, there can be multiple yield surfaces in the flow, which will make the problem more difficult to solve.

Our problem is similar in geometrical configuration to that considered by Chang and Wang [21] and Xie *et al.* [25]. EO flow of a viscoplastic material, modeled as either Bingham plastic or Casson fluid, through a slit channel bounded by two parallel flat plates that rotate about an axis perpendicular to themselves is considered. The zeta potentials on the upper and lower walls are assumed to be so small that the linearized Poisson–Boltzmann equation can be used to determine the electric potential distribution. For simplicity, we also assume negligible effects due to a near-wall depletion layer. This assumption is reasonable when the EDL is thick enough to encapsulate a depletion layer, if any. The problem formulation is described in further detail in Sec. 2. Analytical solutions for two limiting cases are deduced in Sec. 3, which may be used to check the accuracy of our numerical method. The numerical algorithm consisting of finite-differencing and iterative processes is detailed in Sec. 4. Finally, numerical results and discussions are presented in Sec. 5. We shall in particular look into how the velocity profiles and flow rates may change differently, depending on the viscoplastic model, the yield stress, and the rotation speed.

2 Problem formulation

The present problem is to consider EO flow of a viscoplastic material in a parallel-plate channel that rotates about an axis perpendicular to the two parallel plates, which are at a distance of $2h$ apart. As is shown in Fig. 1, a right-handed Cartesian coordinate system is introduced such that the origin is located at a midpoint between the two plates. The channel rotates at a constant angular velocity Ω about an axis parallel to z. The two walls at $z = \pm h$ are charged with the same uniform zeta potential ζ_0. Primary or axial flow occurs in the x-direction, as a result of electrokinetic pumping due to an applied steady electric field E_x in this direction. Meanwhile, secondary or transverse flow

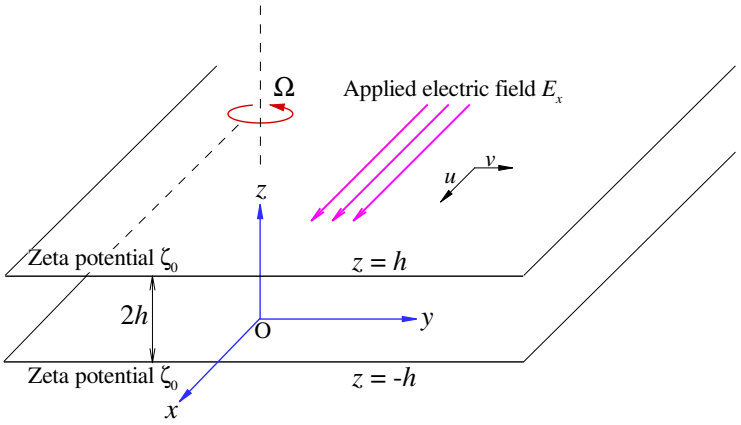

Figure 1: Schematic diagram of the problem: electro-osmotic flow through a parallel-plate channel of height $2h$ rotating about the z-axis with angular velocity Ω. A steady electric field is applied along the x-axis.

happens in the y-direction, as driven by the Coriolis force due to the system rotation.

Assuming steady and fully-developed flow, the variables (stress, velocity, and electric potential) are all functions of z only, and by virtue of symmetry, it suffices to consider the upper half of the channel ($0 \leq z \leq h$) in the following analysis.

For simplicity, it is assumed that there is no pressure gradient (except the one to balance the centrifugal force) in the flow field. It is further assumed that the Rossby number is so low that the nonlinear inertia can be ignored. Ignoring gravity as well, the Cauchy momentum equation for the rotating flow can be written as

$$2\rho\vec{\Omega} \times \vec{u} = \nabla \cdot \boldsymbol{\tau} + \rho_e \vec{E}, \tag{1}$$

where $\boldsymbol{\tau}$ is the stress tensor, $\vec{u} = (u, v, 0)$ is the velocity vector seen in the rotating frame with u and v being the axial and transverse velocity components, $\vec{\Omega} = (0, 0, \Omega)$ is the rotation vector, $\vec{E} = (E_x, 0, 0)$ is the applied electric field, ρ is the fluid density, and ρ_e is the free charge density in the fluid. It is clear from the equation that the flow results from a balance between viscous stress, electric body force ($\rho_e \vec{E}$) and Coriolis force ($2\rho\vec{\Omega} \times \vec{u}$).

The electric potential $\psi(z)$ in the electric double layer (EDL) is governed by the

Poisson equation:

$$\frac{\mathrm{d}^2\psi}{\mathrm{d}z^2} = -\frac{\rho_e}{\epsilon}, \tag{2}$$

where ϵ is the dielectric permittivity of the electrolyte. With the assumptions of a symmetric electrolyte of valence Z and a Boltzmann distribution of ions within the EDL, the relation between the free charge density ρ_e and the electric potential is given by

$$\rho_e = -2Zen_\infty \sinh\left(\frac{Ze\psi}{k_BT}\right), \tag{3}$$

in which e is the fundamental charge, n_∞ is the bulk electric concentration, k_B is the Boltzmann constant, and T is the absolute temperature. Here we invoke the well-known Debye–Hückel approximation on assuming a very small potential, i.e., $Ze\psi/k_BT \ll 1$ so that $\sinh(Ze\psi/k_BT) \approx Ze\psi/k_BT$. This approximation, together with Eqs. (2) and (3), gives the linearized Poisson–Boltzmann (PB) equation

$$\frac{\mathrm{d}^2\psi}{\mathrm{d}z^2} = \kappa^2\psi, \tag{4}$$

where $\kappa = (2Z^2e^2n_\infty/\epsilon k_BT)^{1/2}$ is the Debye parameter, or the reciprocal of the Debye shielding thickness of the EDL. The solution of the PB equation can be readily obtained as

$$\psi(z) = \zeta_0 \frac{\cosh(\kappa z)}{\cosh(\kappa h)} \quad \text{for } 0 \le z \le h, \tag{5}$$

upon using the boundary condition $\psi = \zeta_0$ at the upper plate ($z = h$). In a dimensionless form, the potential distribution can be written as

$$\hat{\psi}(\hat{z}) = \frac{\cosh(\hat{\kappa}\hat{z})}{\cosh(\hat{\kappa})} \quad \text{for } 0 \le \hat{z} \le 1, \tag{6}$$

where $\hat{\psi} = \psi/\zeta_0$, $\hat{z} = z/h$, $\hat{\kappa} = \kappa h$. From Eqs. (2) and (4), the free charge density is given by

$$\rho_e = -\epsilon\kappa^2\psi = -\epsilon\kappa^2\zeta_0 \frac{\cosh(\kappa z)}{\cosh(\kappa h)}. \tag{7}$$

To close the problem, we need to specify a constitutive equation to relate stress and shear rate. Here, two kinds of viscoplastic materials are considered: Bingham plastic and Casson fluid. The Bingham plastic model is

$$\begin{cases} \boldsymbol{\tau} = [\mu_0 + \tau_0/|\dot{\gamma}|]\,\dot{\boldsymbol{\gamma}} & \text{for } |\tau| > \tau_0 \\ \dot{\boldsymbol{\gamma}} = 0 & \text{for } |\tau| \le \tau_0 \end{cases}, \tag{8}$$

while the Casson model is

$$\begin{cases} \boldsymbol{\tau} = \left[\mu_0^{1/2} + (\tau_0/|\dot{\gamma}|)^{1/2}\right]^2 \dot{\boldsymbol{\gamma}} & \text{for } |\tau| > \tau_0 \\ \dot{\boldsymbol{\gamma}} = 0 & \text{for } |\tau| \leq \tau_0 \end{cases}, \tag{9}$$

where $\boldsymbol{\tau}$ and $\dot{\boldsymbol{\gamma}}$ are, respectively, the stress tensor and the rate-of-deformation tensor. Their magnitudes are given by $|\tau| = [(\boldsymbol{\tau} : \boldsymbol{\tau})/2]^{1/2}$ and $|\dot{\gamma}| = [(\dot{\boldsymbol{\gamma}} : \dot{\boldsymbol{\gamma}})/2]^{1/2}$. The two rheological parameters τ_0 and μ_0 are the yield stress and the plastic viscosity, respectively. If the yield stress is identically zero, $\tau_0 \equiv 0$, the Bingham and Casson models will both reduce to the Newtonian model. The presence of a yield stress imposes a threshold for the motion of the material: sheared or unsheared, depending on whether or not the stress is higher in magnitude than the yield stress. The flow domain is accordingly divided into sheared and unsheared regions. The material may flow like a viscous fluid in the former, and may be static or move like a rigid body in the latter.

In the sheared or yielded region, where $|\tau| > \tau_0$, the constitutive equation can be written in component form as follows:

$$\tau_{xz} = \mu \frac{\mathrm{d}u}{\mathrm{d}z}, \qquad \tau_{yz} = \mu \frac{\mathrm{d}v}{\mathrm{d}z}, \tag{10}$$

in which the effective viscosity μ is

$$\mu_{\mathrm{Bn}} = \mu_0 + \frac{\tau_0}{|\dot{\gamma}|} \quad \text{for Bingham plastic,} \tag{11}$$

or

$$\mu_{\mathrm{Ca}} = \left[\mu_0^{1/2} + \left(\frac{\tau_0}{|\dot{\gamma}|}\right)^{1/2}\right]^2 \quad \text{for Casson fluid,} \tag{12}$$

and

$$|\tau| = \sqrt{\tau_{xz}^2 + \tau_{yz}^2} \quad \text{and} \quad |\dot{\gamma}| = \sqrt{\left(\frac{\mathrm{d}u}{\mathrm{d}z}\right)^2 + \left(\frac{\mathrm{d}v}{\mathrm{d}z}\right)^2}. \tag{13}$$

In the unsheared or unyielded region, where $|\tau| \leq \tau_0$, the condition of zero shear rate implies

$$\frac{\mathrm{d}u}{\mathrm{d}z} = \frac{\mathrm{d}v}{\mathrm{d}z} = 0. \tag{14}$$

Alternatively, one can take the effective viscosity to be infinite in the unsheared region.

Let us introduce the following scales for the stress and velocity:

$$\tau_E = -\epsilon\kappa\zeta_0 E_x, \quad U_s = -\epsilon\zeta_0 E_x/\mu_0, \tag{15}$$

by which the following normalized variables (distinguished by overhead carets) can be defined:

$$(\hat{u}, \hat{v}) = (u, v)/U_s, \quad (\hat{\tau}_{xz}, \hat{\tau}_{yz}, \hat{\tau}_0) = (\tau_{xz}, \tau_{yz}, \tau_0)/\tau_E. \tag{16}$$

Note that U_s is similar in form to the Helmholtz–Smoluchowski velocity. On substituting Eq. (7) and the normalized variables into Eq. (1), we get the following dimensionless component form of the Cauchy momentum equation:

$$-\omega\hat{v} = \hat{\kappa}\frac{\mathrm{d}\hat{\tau}_{xz}}{\mathrm{d}\hat{z}} + \hat{\kappa}^2\hat{\psi}, \tag{17}$$

$$\omega\hat{u} = \hat{\kappa}\frac{\mathrm{d}\hat{\tau}_{yz}}{\mathrm{d}\hat{z}}, \tag{18}$$

where ω is the rotation parameter

$$\omega = \frac{2\rho h^2\Omega}{\mu_0}, \tag{19}$$

which is also known as the inverse Ekman number.

In terms of the normalized variables, the constitutive equations for the sheared region ($|\hat{\tau}| > \hat{\tau}_0$) are

$$\hat{\tau}_{xz} = \left(\frac{\hat{\mu}}{\hat{\kappa}}\right)\frac{\mathrm{d}\hat{u}}{\mathrm{d}\hat{z}}, \quad \hat{\tau}_{yz} = \left(\frac{\hat{\mu}}{\hat{\kappa}}\right)\frac{\mathrm{d}\hat{v}}{\mathrm{d}\hat{z}}, \tag{20}$$

where the normalized effective viscosity $\hat{\mu}$ is given by either

$$\hat{\mu}_{\mathrm{Bn}} = 1 + \frac{\hat{\kappa}\hat{\tau}_0}{|\hat{\dot{\gamma}}|} \quad \text{for Bingham plastic,} \tag{21}$$

or

$$\hat{\mu}_{\mathrm{Ca}} = \left[1 + \left(\frac{\hat{\kappa}\hat{\tau}_0}{|\hat{\dot{\gamma}}|}\right)^{1/2}\right]^2 \quad \text{for Casson fluid,} \tag{22}$$

in which

$$|\hat{\tau}| = \sqrt{\hat{\tau}_{xz}^2 + \hat{\tau}_{yz}^2} \quad \text{and} \quad |\hat{\dot{\gamma}}| = \sqrt{\left(\frac{\mathrm{d}\hat{u}}{\mathrm{d}\hat{z}}\right)^2 + \left(\frac{\mathrm{d}\hat{v}}{\mathrm{d}\hat{z}}\right)^2}. \tag{23}$$

When the yield stress is zero, the plastic viscosity becomes the Newtonian viscosity:

$$\lim_{\hat{\tau}_0 \to 0} \hat{\mu}_{\mathrm{Bn}} = \lim_{\hat{\tau}_0 \to 0} \hat{\mu}_{\mathrm{Ca}} = 1. \tag{24}$$

Again, in the unsheared region ($|\hat{\tau}| \leq \hat{\tau}_0$),

$$\frac{\mathrm{d}\hat{u}}{\mathrm{d}\hat{z}} = \frac{\mathrm{d}\hat{v}}{\mathrm{d}\hat{z}} = 0 \qquad \text{or} \qquad \hat{\mu} = \infty. \tag{25}$$

3 Limiting cases

Let us first review two limiting cases, for which analytical solutions can be deduced. We shall use these analytical solutions to check the accuracy of our numerical method, as is presented in Fig. 2.

3.1 EO flow of viscoplastic material in a non-rotating channel

Ng and Qi [12] have studied EO flow of viscoplastic materials in a non-rotating parallel-plate channel with arbitrary wall potentials. Let us revisit the problem here, considering a small wall potential only.

Without rotation ($\omega = 0$), the secondary flow vanishes exactly or $\hat{v} \equiv 0$. Also, Eqs. (6) and (17) give

$$\frac{\mathrm{d}\hat{\tau}_{xz}}{\mathrm{d}\hat{z}} = -\hat{\kappa}\frac{\cosh(\hat{\kappa}\hat{z})}{\cosh(\hat{\kappa})}, \tag{26}$$

from which we get the following stress distribution, after using the symmetry condition of zero stress at $\hat{z} = 0$,

$$\hat{\tau}_{xz} = -\frac{\sinh(\hat{\kappa}\hat{z})}{\cosh(\hat{\kappa})}. \tag{27}$$

Note that this stress distribution is valid for any fluid, Newtonian or non-Newtonian. The stress is maximum in magnitude at the wall ($\hat{z} = 1$), given by

$$\hat{\tau}_c = \tanh(\hat{\kappa}). \tag{28}$$

When the electric forcing is so small that $\hat{\tau}_c < \hat{\tau}_0$, the material will remain static. Flow will happen only when the forcing is strong enough to have the wall stress larger in magnitude than the yield stress, $\hat{\tau}_c > \hat{\tau}_0$. When this happens, because of the monotonicity of the stress distribution, there is one and only one yield surface in the flow. The yield surface is located at $\hat{z} = \hat{z}_0$, which can be readily found as

$$\hat{z}_0 = \frac{1}{\hat{\kappa}}\sinh^{-1}\left[\hat{\tau}_0\cosh(\hat{\kappa})\right] \quad \text{where } \hat{\tau}_0 < \tanh(\hat{\kappa}). \tag{29}$$

It follows that the flow is unsheared (hence a uniform flow) in the center region $0 \le \hat{z} < \hat{z}_0$, and is sheared in the near-wall region $\hat{z}_0 < \hat{z} \le 1$.

As the velocity gradient is negative in the upper half of the channel, the magnitude of the shear rate is

$$|\hat{\dot{\gamma}}| = \left|\frac{\mathrm{d}\hat{u}}{\mathrm{d}\hat{z}}\right| = -\frac{\mathrm{d}\hat{u}}{\mathrm{d}\hat{z}}. \tag{30}$$

3.1.1 Bingham plastic

For a Bingham plastic, the velocity in the sheared region can be found from Eq. (20) after substituting Eqs. (21) and (27):

$$\begin{aligned} \hat{u}_{\mathrm{s}}(\hat{z}) &= \hat{\kappa}\int_{\hat{z}}^{1}\left[\frac{\sinh(\hat{\kappa}\hat{z})}{\cosh(\hat{\kappa})} - \hat{\tau}_0\right]\mathrm{d}\hat{z} \\ &= 1 - \hat{\kappa}\hat{\tau}_0\,(1-\hat{z}) - \cosh(\hat{\kappa}\hat{z})/\cosh(\hat{\kappa}) \qquad \text{for } \hat{z}_0 < \hat{z} \le 1. \end{aligned} \tag{31}$$

In the unsheared region, the plug-like flow has a uniform velocity:

$$\begin{aligned} \hat{u}_{\mathrm{us}} &= \hat{u}_{\mathrm{s}}(\hat{z}_0) \\ &= 1 - \hat{\kappa}\hat{\tau}_0\,(1-\hat{z}_0) - \cosh(\hat{\kappa}\hat{z}_0)/\cosh(\hat{\kappa}) \qquad \text{for } 0 \le \hat{z} < \hat{z}_0, \end{aligned} \tag{32}$$

where $\hat{z}_0$ is given by Eq. (29).

3.1.2 Casson fluid

Likewise, the velocity profile for a Casson fluid can be found from Eqs. (20), (22) and (27):

$$\hat{u}_{\mathrm{s}}(\hat{z}) = 1 - \cosh(\hat{\kappa}\hat{z})/\cosh(\hat{\kappa}) + \hat{\kappa}\hat{\tau}_0(1-\hat{z}) - 2\hat{\kappa}I(\hat{z}) \quad \text{for } \hat{z}_0 < \hat{z} \le 1, \tag{33}$$

and $\hat{u}_{\mathrm{us}} = \hat{u}_{\mathrm{s}}(\hat{z}_0)$ for $0 \le \hat{z} < \hat{z}_0$, where

$$I(\hat{z}) = \int_{\hat{z}}^{1}\left[\frac{\hat{\tau}_0\sinh(\hat{\kappa}\hat{z})}{\cosh(\hat{z})}\right]^{\frac{1}{2}}\mathrm{d}\hat{z}, \tag{34}$$

which can be numerically evaluated, say by Simpson's rule.

3.2 Rotating EO flow of Newtonian fluid

Chang and Wang [21] and Ng and Qi [22] already developed solutions for EO flow of Newtonian fluid in a rotating slit channel. Let us briefly re-examine the problem here, deriving solutions in terms of the present notation.

When the yield stress is zero, $\hat{\tau} = 0$, the momentum equations simplify to

$$-\omega\hat{v}_0 = \frac{\mathrm{d}^2\hat{u}_0}{\mathrm{d}\hat{z}^2} + \hat{\kappa}^2\frac{\cosh(\hat{\kappa}\hat{z})}{\cosh(\hat{\kappa})}, \tag{35}$$

$$\omega\hat{u}_0 = \frac{\mathrm{d}^2\hat{v}_0}{\mathrm{d}\hat{z}^2}, \tag{36}$$

where we have used the subscript "0" to denote the case of zero yield stress. The general solution to these equations can be expressed as

$$\hat{u}_0(\hat{z}) = -A\cosh(\hat{\kappa}\hat{z})/\cosh(\hat{\kappa}) + 2C_1\cosh(\eta\hat{z})\cos(\eta\hat{z}) + 2C_2\sinh(\eta\hat{z})\sin(\eta\hat{z}), \tag{37}$$

$$\hat{v}_0(\hat{z}) = -B\cosh(\hat{\kappa}\hat{z})/\cosh(\hat{\kappa}) + 2C_1\sinh(\eta\hat{z})\sin(\eta\hat{z}) - 2C_2\cosh(\eta\hat{z})\cos(\eta\hat{z}), \tag{38}$$

where $\eta = (\omega/2)^{1/2}$,

$$A = \frac{\hat{\kappa}^4}{\hat{\kappa}^4 + \omega^2}, \quad \text{and} \quad B = \frac{\omega\hat{\kappa}^2}{\hat{\kappa}^4 + \omega^2}. \tag{39}$$

Using the no-slip condition at the wall, the coefficients $C_{1,2}$ can be determined as follows:

$$C_1 = \frac{A\cosh(\eta)\cos(\eta) + B\sinh(\eta)\sin(\eta)}{\cosh(2\eta) + \cos(2\eta)}, \tag{40}$$

$$C_2 = \frac{A\sinh(\eta)\sin(\eta) - B\cosh(\eta)\cos(\eta)}{\cosh(2\eta) + \cos(2\eta)}. \tag{41}$$

Integrating the velocities across the channel gives the primary and secondary flow rates:

$$\begin{aligned}\hat{q}_{0x} &= 2\int_0^1 \hat{u}_0(\hat{z})\ \mathrm{d}\hat{z} \\ &= -\frac{2A\tanh(\hat{\kappa})}{\hat{\kappa}} + \frac{2}{\eta}\left[(C_1 - C_2)\sinh(\eta)\cos(\eta) + (C_1 + C_2)\cosh(\eta)\sin(\eta)\right],\end{aligned} \tag{42}$$

$$\begin{aligned}\hat{q}_{0y} &= 2\int_0^1 \hat{v}_0(\hat{z})\ \mathrm{d}\hat{z} \\ &= -\frac{2B\tanh(\hat{\kappa})}{\hat{\kappa}} + \frac{2}{\eta}\left[(-C_1 - C_2)\sinh(\eta)\cos(\eta) + (C_1 - C_2)\cosh(\eta)\sin(\eta)\right]\end{aligned} \tag{43}$$

The stress components are also found as follows:

$$\begin{aligned}\hat{\tau}_{0xz} &= \frac{1}{\hat{\kappa}}\frac{\mathrm{d}\hat{u}_0}{\mathrm{d}\hat{z}} \\ &= -A\frac{\sinh(\hat{\kappa}\hat{z})}{\cosh(\hat{\kappa})} + \frac{2\eta}{\hat{\kappa}}\left[(-C_1 + C_2)\cosh(\eta\hat{z})\sin(\eta\hat{z})\right. \\ &\quad \left. + (C_1 + C_2)\sinh(\eta\hat{z})\cos(\eta\hat{z})\right],\end{aligned} \tag{44}$$

$$\begin{aligned}\hat{\tau}_{0yz} &= \frac{1}{\hat{\kappa}}\frac{\mathrm{d}\hat{v}_0}{\mathrm{d}\hat{z}} \\ &= -B\frac{\sinh(\hat{\kappa}\hat{z})}{\cosh(\hat{\kappa})} + \frac{2\eta}{\hat{\kappa}}\left[(C_1 + C_2)\cosh(\eta\hat{z})\sin(\eta\hat{z})\right. \\ &\quad \left. + (C_1 - C_2)\sinh(\eta\hat{z})\cos(\eta\hat{z})\right].\end{aligned} \tag{45}$$

4 Numerical solution method

One can reason that, by comparing Eq. (27) with Eqs. (44) and (45), the stress field can be materially modified by the system rotation. With rotation, the stress magnitude may no longer be a monotonous function of $\hat{z}$. As will be shown later, there can be a local maximum in the distribution of $|\hat{\tau}|$. Hence, in principle, there can be more than one position where the stress magnitude is equal to the yield stress, implying that there can be multiple sheared or unsheared regions in the rotating flow of a viscoplastic material.

To avoid this complicated situation, let us assume that the material under consideration has a relatively small yield stress. This will limit the yield surface to be located at a point in the center region, within which the stress distribution still maintains a monotonous increasing trend with $\hat{z}$. In other words, we consider only cases in which the stress has a monotonous distribution in the unyielded region. This will also ensure a one-to-one relationship between yield stress and position of the yield surface.

Normally, one would first specify the yield stress, as this is one of the fluid properties, before solving the problem for the velocity and stress components. However, this way of finding solutions for a yield-stress material could be rather cumbersome as it would involve in each iteration the adjustment of the yield surface position.

In this work, we shall adopt a reverse approach: first prescribe a value for the yield surface position, and then solve for the corresponding yield stress. This is legitimate as long as there exists a unique mapping between the two quantities. This is why we need to assume a relatively small yield stress, as explained above. We remark that this is not an unrealistic assumption, because many fluids of practical interest (e.g., blood) have indeed a small yield stress.

The reverse approach will enable us to separate in advance the domain into the sheared and unsheared regions, where different governing equations are to be applied. The ensuing numerical analysis can be performed without the need for the adjustment of the yield surface position in each iteration.

To facilitate the seeking of solution by iteration, let us put the unsteady term back to

the momentum equations. In the sheared region ($\hat{z}_0 < \hat{z} \leq 1$), the momentum equations read as follows:

$$\frac{\partial \hat{u}}{\partial \hat{t}} - \omega \hat{v} = \frac{\partial}{\partial \hat{z}} \left(\hat{\mu} \frac{\partial \hat{u}}{\partial \hat{z}} \right) + \hat{\kappa}^2 \hat{\psi}, \tag{46}$$

$$\frac{\partial \hat{v}}{\partial \hat{t}} + \omega \hat{u} = \frac{\partial}{\partial \hat{z}} \left(\hat{\mu} \frac{\partial \hat{v}}{\partial \hat{z}} \right), \tag{47}$$

where the effective viscosity $\hat{\mu}$ is given by Eq. (21) for Bingham plastic, or Eq. (22) for Casson fluid. The problem is now discretized, and an iterative scheme is to be devised through the local acceleration term, which should diminish toward zero to achieve convergence to the solution.

The sheared region ($\hat{z}_0 < \hat{z} \leq 1$) is discretized into a number of evenly spaced points, i.e., $z_i = \hat{z}_0 + (i-1)\,\Delta z$ $(i = 1, 2, \cdots, N, N+1)$ with the grid spacing $\Delta z = (1 - \hat{z}_0)/N$. The axial and transverse velocity components at $\hat{z} = z_i$ are denoted by u_i and v_i. Using forward-time central-space difference, the two momentum equations above can be approximated by the following difference equations:

$$\frac{u_i^{(n+1)} - u_i^{(n)}}{\Delta t} - \omega v_i^{(n)} = \frac{\hat{\mu}_{i+1/2}^{(n)} \left(u_{i+1}^{(n)} - u_i^{(n)} \right) - \hat{\mu}_{i-1/2}^{(n)} \left(u_i^{(n)} - u_{i-1}^{(n)} \right)}{\Delta z^2} + \hat{\kappa}^2 \hat{\psi}_i, \tag{48}$$

$$\frac{v_i^{(n+1)} - v_i^{(n)}}{\Delta t} + \omega u_i^{(n)} = \frac{\hat{\mu}_{i+1/2}^{(n)} \left(v_{i+1}^{(n)} - v_i^{(n)} \right) - \hat{\mu}_{i-1/2}^{(n)} \left(v_i^{(n)} - v_{i-1}^{(n)} \right)}{\Delta z^2}, \tag{49}$$

where n denotes the time level and Δt is the time step such that $\hat{t} = n\Delta t$, and $\hat{\mu}_{i\pm1/2} = \left(\hat{\mu}_{i\pm1} + \hat{\mu}_i\right)/2$. Here, the time step is a parameter that can be used to control the rate of convergence of the iterative process. To compute the effective viscosity, we need the magnitude of the shear rate, which can be determined using second-order central difference as follows:

$$|\hat{\dot{\gamma}}_i| = \sqrt{\left(\frac{u_{i+1} - u_{i-1}}{2\Delta z} \right)^2 + \left(\frac{v_{i+1} - v_{i-1}}{2\Delta z} \right)^2}. \tag{50}$$

The flow is to satisfy continuity of velocity gradients and no-slip conditions at the yield surface and the wall, respectively. Accurate to the second order, these boundary conditions are

$$\frac{-3u_1 + 4u_2 - u_3}{2\Delta z} = \frac{-3v_1 + 4v_2 - v_3}{2\Delta z} = 0 \quad \text{at } \hat{z} = z_1, \tag{51}$$

$$u_{N+1} = v_{N+1} = 0 \quad \text{at } \hat{z} = z_{N+1}. \tag{52}$$

In the unsheared region ($0 \leq \hat{z} < \hat{z}_0$), the velocity gradients are zero, implying constant velocity components in this region. Denoting the axial and transverse velocity components by $\hat{u}_{\rm us}$ and $\hat{v}_{\rm us}$, we may get the stress components in the unsheared region by integrating Eqs. (17) and (18):

$$\hat{\tau}_{xz} = -\left(\frac{\omega \hat{v}_{\rm us}}{\hat{\kappa}}\right)\hat{z} - \frac{\sinh(\hat{\kappa}\hat{z})}{\cosh(\hat{\kappa})}, \tag{53}$$

$$\hat{\tau}_{yz} = \left(\frac{\omega \hat{u}_{\rm us}}{\hat{\kappa}}\right)\hat{z}, \tag{54}$$

where the symmetry condition of zero stress at the centerline ($\hat{z} = 0$) has been used. At the yield surface ($\hat{z} = z_1$), the continuity of velocity and stress implies

$$\hat{u}_{\rm us} = u_1, \quad \hat{v}_{\rm us} = v_1, \tag{55}$$

and

$$|\hat{\tau}|_{\hat{z}=z_1} = \sqrt{\hat{\tau}_{xz}^2 + \hat{\tau}_{yz}^2}\Big|_{\hat{z}=z_1} = \hat{\tau}_0. \tag{56}$$

After substitution, the equation above can be written as

$$\hat{\tau}_0 = \sqrt{\left[\frac{\omega v_1 z_1}{\hat{\kappa}} + \frac{\sinh(\hat{\kappa} z_1)}{\cosh(\hat{\kappa})}\right]^2 + \left(\frac{\omega u_1 z_1}{\hat{\kappa}}\right)^2}. \tag{57}$$

To kick off the iteration, we use the solution for Newtonian fluid as the initial guess values: $\hat{\mu}_i^{(0)} = 1$, $\hat{\tau}_0^{(0)} = 0$, $u_i^{(0)} = \hat{u}_0(\hat{z} = z_i)$ and $v_i^{(0)} = \hat{v}_0(\hat{z} = z_i)$, where $\hat{u}_0(\hat{z})$ and $\hat{v}_0(\hat{z})$ are given in Eqs. (37) and (38). For the given input parameters $\hat{\kappa}$, ω and $\hat{z}_0$, we may get from Eqs. (48) and (49), in an explicit manner, the next-time-level values for the velocities u_i and v_i where $i = 2, \cdots, N$. The velocities (u_{N+1}, v_{N+1}) are zero, while (u_1, v_1) are determined from Eq. (51). The magnitude of the shear rate, and the yield stress can then be updated using Eqs. (50) and (57). The effective viscosity, given by either Eq. (21) or (22), can be updated as well. With these updated values, we may start another round of time advancement. These iterative steps are to be repeated until the maximum relative difference between values of axial and transverse velocities at two consecutive time levels is below a prescribed tolerance level.

5 Discussion

We choose values of the input parameters based on the following consideration: the permittivity of the electrolyte solution $\epsilon = 709 \times 10^{-12}$ F/m, the half-channel-height $h \sim 100$ μm, the constant electric field $E \sim 5 \times 10^4$ V/m, and the wall potential $\zeta_0 \sim -20$ mV. The shielding depth of the EDL (κ^{-1}) is typically in a range of 10 nm to 10 μm. Therefore, $\hat{\kappa} \geq O(10)$. In all the cases presented below, a fixed value of $\hat{\kappa} = 10$ is considered. In addition, the magnitude of yield stress τ_0, comparable to that of human blood, is of the order 5 mPa at a room temperature, corresponding to a normalized value ($\hat{\tau}_0 = \tau_0/\tau_{\rm E}$) of the order 0.1. The rotation speed can vary over a wide range, depending on the application. As in Chang and Wang [21] and Ng and Qi [22], a rotation rate in the range of $0 \leq \omega < 100$ will be considered.

5.1 Velocity and stress profiles

We first show in Fig. 2 the profiles of axial velocity $\hat{u}(\hat{z})$, transverse velocity $\hat{v}(\hat{z})$ and stress magnitude $|\hat{\tau}|(\hat{z})$ for EO flow of Newtonian, Bingham and Casson fluids under a system rotation of speed $\omega = 0$, 5, 10, 50. For the Bingham and Casson fluids, a yield stress of $\hat{\tau}_0 = 0.05$ is considered. The position of the yield surface, $\hat{z}_0$, where the stress magnitude equals the yield stress, is denoted by a cross bar in the velocity distributions for the Bingham and Casson fluids, as shown in Figs. 2(d, e, g, h). To the left of the yield surface is the unsheared region where the flow is uniform or plug-like.

Also shown in Fig. 2 is a comparison of results generated by our numerical model (solid lines) and those generated by the analytical models (circles) as described above for rotating EO flow of Newtonian fluid and EO flow of Bingham and Casson fluids in a non-rotating channel. Clearly, the two sets of results are in close agreement with each other. This provides some support to the accuracy of our numerical model.

In the case of Newtonian fluid, the results are essentially the same as those presented previously by Chang and Wang [21], as is expected. Note that there is a change in the flow structure as the rotation speed varies from $\omega = 0$ to $\omega \gg 1$. In the absence of

rotation, the velocity profile is that of classical EO flow: the flow is sheared in a near-wall region encompassing the EDL, and has a uniform velocity, known as the Helmholtz–Smoluchowski velocity, in the core region where the electric forcing is zero. The system rotation is to reduce the axial velocity in the core region. For an intermediate value of ω, a reflux (negative $\hat{u}$) of axial flow may even happen in the center region. At the limiting $\omega \gg 1$, an Ekman–EDL layer shows up near the wall, while an inviscid geostrophic core shows up in the interior. The Ekman–EDL layer results from a balance between viscous, electric and Coriolis forces [22]. This is a thin layer formed near the wall when both $\hat{\kappa}$ and ω are large. The geostrophic core is essentially a non-viscous region where the Coriolis force can only be balanced by pressure gradient, if any. In the present problem, the pressure gradient is zero in both the axial and transverse directions, and hence the flow in these directions will tend to a zero velocity in the center region as $\omega \to \infty$.

The change in flow structure also leads to a change in the stress distribution as ω varies. At $\omega = 0$, the velocity and stress are all monotonic functions of $\hat{z}$. When $\omega \neq 0$, the emergence of the Ekman–EDL layer causes a non-monotonic variation of the stress magnitude near the wall. The stress magnitude has a local minimum near the point where the axial velocity is maximum in magnitude. Such a non-monotonic variation of the stress magnitude also shows up in the case of a viscoplastic material. Figure 2 shows that the introduction of a yield stress into the shearing does not materially change the stress magnitude distribution as a function of the rotation speed. In sharp contrast, the presence of a yield stress may dramatically change the velocity profiles. A direct consequence of the yield stress is a plug flow in the interior. At $\omega = 0$, the plug flow velocity of Bingham plastic or Casson fluid is smaller than the Helmholtz–Smoluchowski velocity of the corresponding Newtonian fluid flow. Because of the square roots in the constitutive relationship, a Casson fluid is subject to a larger reducing effect of the yield stress on the plug flow velocity, as has been found previously by Ng [11] and Ng and Qi [12]. A yield stress as small as $\hat{\tau}_0 = 0.05$ is already large enough to result in a plug flow velocity that is 20% and 60% smaller than the Helmholtz–Smoluchowski velocity, for Bingham and Casson fluids, respectively; see Figs. 2(d, g). When $\omega \neq 0$, the yield stress will, however, tend to lessen the decreasing effect of the system rotation on the axial flow velocity. This is especially true for Casson fluid. On comparing Figs. 2(a) and 2(g), it

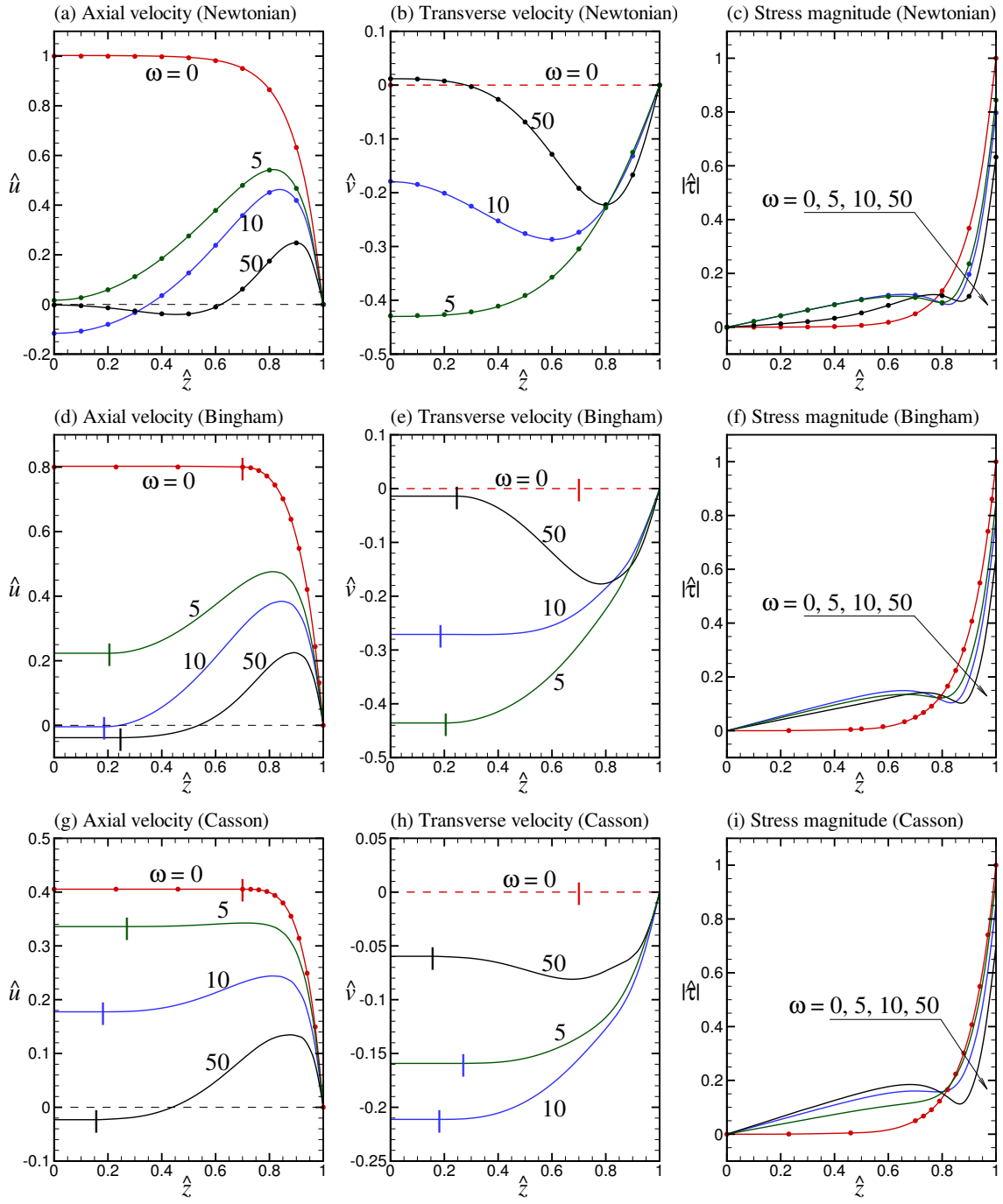

Figure 2: Profiles of axial velocity $\hat{u}(\hat{z})$, transverse velocity $\hat{v}(\hat{z})$ and stress magnitude $|\hat{\tau}|(\hat{z})$ for several values of rotation speed ω, where the material is Newtonian fluid in (a–c), Bingham plastic in (d–f), and Casson fluid in (g–i). The yield stress for the latter two materials is $\hat{\tau}_0 = 0.05$. The circles denote analytical solutions and the cross bars denote the position of the yield surface $\hat{z}_0$.

is seen that the change in the flow structure as ω varies is more gradual in the case of Casson fluid than in the case of Newtonian fluid. The overall effect is that the yield stress is to delay the attainment of the geostrophic limit as ω increases. At an intermediate $\omega = 10$, both the axial and transverse velocities for the viscoplastic materials are more uniformly distributed than the Newtonian counterparts. It is possible that, with $\omega \neq 0$, the near-center velocity of a viscoplastic material is higher in magnitude than that of a Newtonian fluid. This is in sharp contrast to what happens when $\omega = 0$.

5.2 Position of yield surface

We next show in Fig. 3 how the position of the yield surface $\hat{z}_0$ may change as a function of the rotation speed ω and the yield stress $\hat{\tau}_0$ for Bingham plastic and Casson fluid. When $\omega = 0$, $\hat{z}_0$ can be determined analytically, as given by Eq. (29), which is independent of whether the material is Bingham plastic or Casson fluid. As is expected, a larger yield stress corresponds to a larger unsheared or plug flow region. System rotation is to diminish this unsheared region, however. In the case of Bingham plastic, the effect of ω on $\hat{z}_0$ is most prominent in the range $0 < \omega < 5$: there is a sharp drop-off of $\hat{z}_0$ as the rotation speed varies slightly from zero. After reaching a minimum, $\hat{z}_0$ may increase, but very mildly, as ω increases toward a large value. In the case of Casson fluid, the sharp decline of $\hat{z}_0$ tends to happen at larger values of ω, especially for large $\hat{\tau}_0$. Also, the decreasing trend of $\hat{z}_0$ may persist even when $\omega \gg 1$. The overall effect is that, at an intermediate ω, $\hat{z}_0$ for Casson fluid can be larger than that for Bingham plastic, but at a larger ω, the opposite can be true. Physically, this implies that, for a finite yield stress, a Casson fluid may maintain a larger unsheared region (compared with Bingham plastic) when the rotation speed is only moderately large. In other words, a Casson fluid is less susceptible to the decreasing effect of the system rotation on the flow when the rotation speed is not too large. This echoes to what has been inferred from Fig. 2, as remarked above.

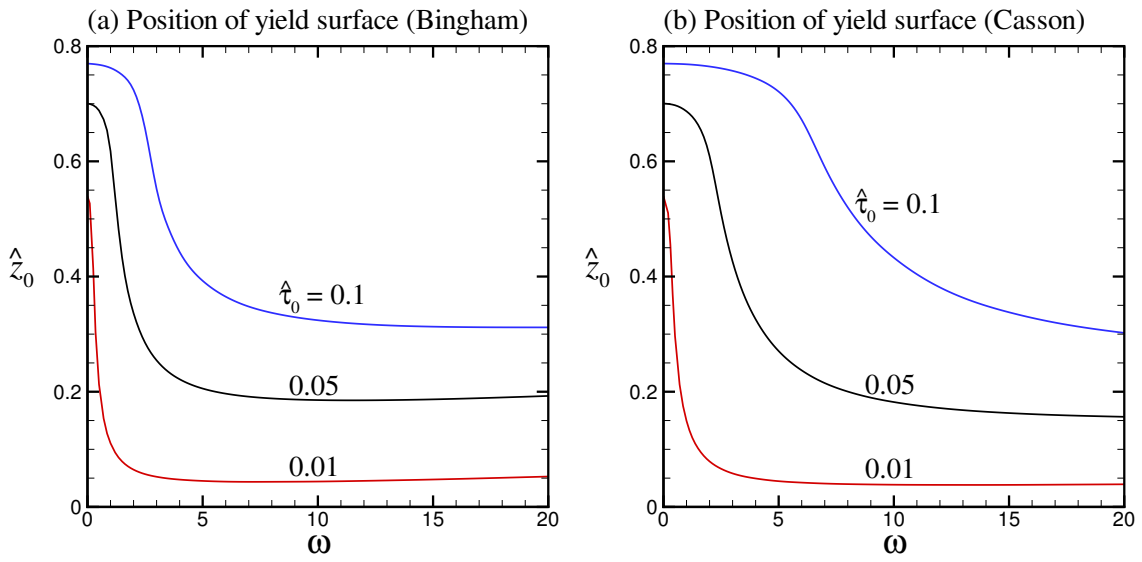

Figure 3: Position of the yield surface $\hat{z}_0$ as a function of rotation speed ω for several values of yield stress $\hat{\tau}_0$, where the material is Bingham plastic in (a), and Casson fluid in (b).

5.3 Flow rate

Figures 4–6 show the flow rates and flow direction as functions of the yield stress and rotation speed for Bingham plastic and Casson fluid. In these figures, the various fluxes and flow direction are computed as follows:

$$\hat{q}_x = 2\int_0^1 \hat{u}\mathrm{d}\hat{z}, \quad \hat{q}_y = 2\int_0^1 \hat{v}\mathrm{d}\hat{z}, \quad \hat{q} = \left(\hat{q}_x^2 + \hat{q}_y^2\right)^{1/2}, \quad \beta = \tan^{-1}(\hat{q}_y/\hat{q}_x). \tag{58}$$

Figures 4 and 5 further reveal how the presence of a yield stress may lessen the decreasing effect of system rotation on the flow, and conversely, how the system rotation may weaken or even reverse the effect of the yield stress. We first point out that, for any yield stress, increasing the rotation speed is always to decrease the axial flow rate; see Figs. 6(a, d). The transverse flow rate may first increase in magnitude as ω increases from 0, but will eventually diminish to zero as $\omega \to \infty$; see Figs. 6(b, e). Despite the non-monotonicity in the transverse flow rate, the resultant flow rate will always decrease monotonically as ω increases, for any yield stress. We also recall that, in the absence of rotation ($\omega = 0$), increasing the yield stress is always to decrease the flow rate. Such decrease in flow rate with increasing yield stress is much more dramatic in the case of

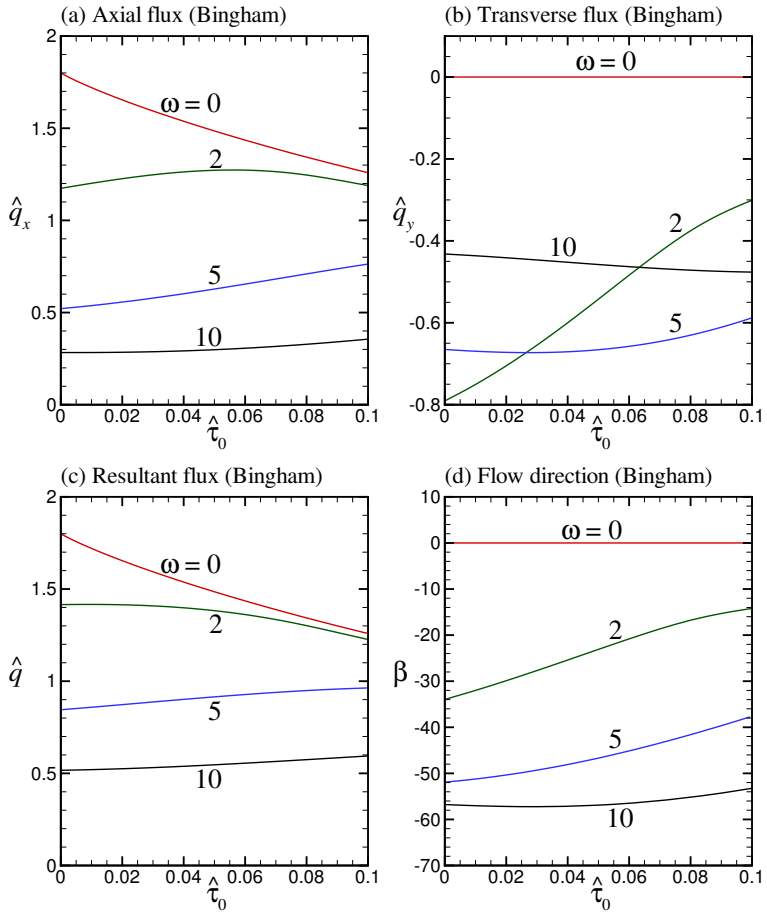

Figure 4: Axial flux $\hat{q}_x$, transverse flux $\hat{q}_y$, resultant flux $\hat{q}$ and flow direction β as functions of yield stress $\hat{\tau}_0$ for several values of rotation speed ω, where the material is Bingham plastic.

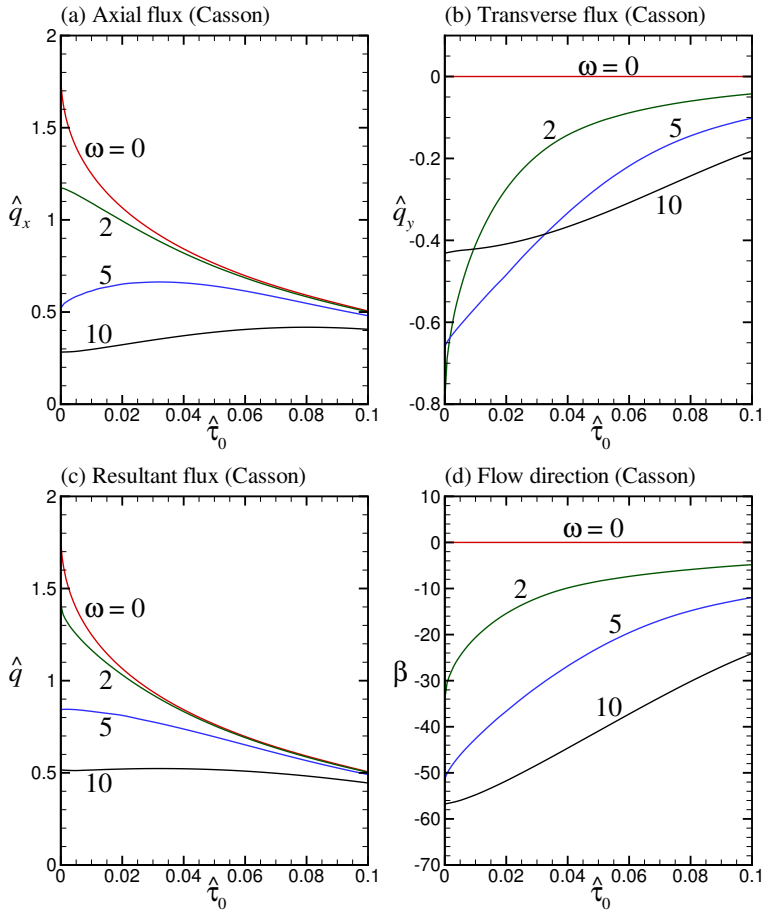

Figure 5: Axial flux $\hat{q}_x$, transverse flux $\hat{q}_y$, resultant flux $\hat{q}$ and flow direction β as functions of yield stress $\hat{\tau}_0$ for several values of rotation speed ω, where the material is Casson fluid.

Casson fluid, as can be seen by comparing the top curves in Figs. 4(a) and 5(a). This is, however, not necessarily true when the rotation speed is not zero. From Figs. 4(a) and 5(a), it is interesting to find that, when $\omega \neq 0$, the axial flow rate does not necessarily decrease with increasing yield stress. For either Bingham plastic or Casson fluid, when ω is sufficiently large, the axial flow rate $\hat{q}_x$ may, to the contrary, increase as the yield stress increases up to a certain value. For example, in the case of Bingham plastic, as $\hat{\tau}_0$ increases from 0 to 0.1, the axial flow rate $\hat{q}_x$ decreases from 1.8 to 1.26 (30% decrease) when $\omega = 0$, but increases from 0.52 to 0.76 (46% increase) when $\omega = 5$; see Fig. 4(a). Such quantitative and qualitative change in the effect of the yield stress owing to the system rotation is manifested even in the resultant flow rate; see Fig. 4(c). One can see from Figs. 4(c) and 5(c) that the system rotation is in general to weaken, if not to reverse, the decreasing effect of the yield stress on the resultant flow rate. As a consequence, the decreasing effect of the system rotation on the flow is also weakened by the presence of a yield stress. For example, in the case of Bingham plastic, as ω increases from 0 to 10, the resultant flow rate $\hat{q}$ drops from 1.8 to 0.52 (71% decrease) when $\hat{\tau}_0 = 0$, but drops only from 1.26 to 0.60 (52% decrease) when $\hat{\tau}_0 = 0.1$; see Fig. 4(c). In the case of Casson fluid, the resultant flow rate drops by an even smaller amount (from 0.51 to 0.44, i.e., 14%) at $\hat{\tau}_0 = 0.1$; see Fig. 5(c). This confirms our earlier finding that the flow of a Casson fluid becomes increasingly unaffected by the system rotation as its yield stress increases. On comparing Figs. 6(a, b) with 6(d, e), one can clearly see that, when $\hat{\tau}_0 = 0.1$, the axial and transverse flow rates of a Casson fluid are much less sensitive to the rotation speed than those of a Bingham plastic.

From Figs. 4(d), 5(d) and 6(c, f), we also see that increasing the yield stress will in general decrease the angle of inclination of the resultant flow with respect to the axial direction. This effect is more pronounced for Casson fluid than Bingham plastic. Hence, for any finite values of ω and $\hat{\tau}_0$, the flow of a Casson fluid is more directed toward the axial direction than the flow of a Bingham plastic.

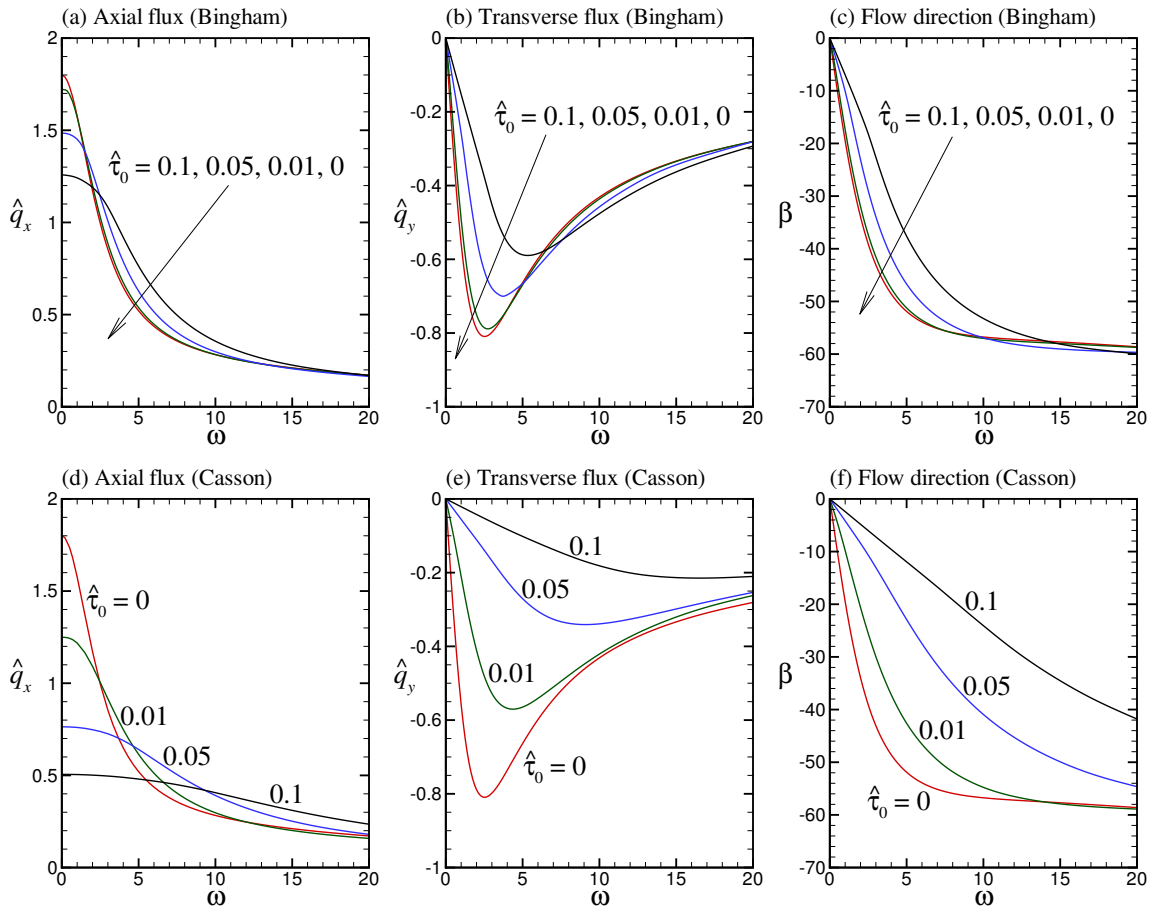

Figure 6: Axial flux $\hat{q}_x$, transverse flux $\hat{q}_y$, and flow direction β as functions of rotation speed ω for several values of yield stress $\hat{\tau}_0$, where the material is Bingham plastic in (a–c), and Casson fluid in (d–f).

6 Concluding remarks

We have developed an iterative numerical scheme to solve the problem of electroosmotic flow of a viscoplastic material modeled as either Bingham plastic or Casson fluid in a parallel-plate channel that rotates about an axis perpendicular to the plates. For a given yield stress, the location of the yield surface together with the velocity and stress components can be found by solving the Cauchy momentum equations, which are approximated by finite differences, by means of an iterative process. We have also looked into numerical results illustrating how the primary and secondary flows are differently affected by the yield stress of the material, depending on the viscoplastic model and the rotation speed.

Some key findings are summarized as follows. First, in the presence of system rotation of sufficiently high speed, the stress distribution can be non-monotonic near the outer edge of the EDL. Therefore, if the material has a yield stress, there is a single yield surface only when the yield stress is not too large. A large yield stress may result in multiple yield surfaces, hence multiple sheared and unsheared regions, in the flow. In this study, only the case of a single yield surface is considered. We leave it to a future study to investigate the case of multiple yield surfaces. Second, the presence of a yield stress may slow down the attainment of the inviscid geostrophic interior as the rotation speed increases toward a large value. This effect is more pronounced for a Casson fluid. Third, for a non-zero rotation speed, the axial flow rate may possibly increase as the yield stress increases. This is in sharp contrast to the case of zero rotation, for which the flow rate can only be decreased by a yield stress. This has led us to conclude that system rotation may weaken or even reverse the decreasing effect of yield stress on the flow. Fourth, larger the yield stress, smaller the decreasing effect of system rotation on the flow rate. The rate and direction of flow of a Casson fluid are much less sensitive to the rotation speed than those of a Bingham plastic of the same yield stress.

Acknowledgments

The work was supported by the Research Grants Council of the Hong Kong Special Administrative Region, China, through Project Nos. HKU 715510E and 17206615, and also by the University of Hong Kong through the Small Project Funding Scheme under Project Code 201309176109.

References

[1] H.A. Stone, A.D. Stroock, A. Ajdari, Engineering flows in small devices: microfluidics toward a lab-on-a-chip, Annu. Rev. Fluid Mech. 36 (2004) 381–411.

[2] F.F. Reuss, Charge-induced flow, Proc. Imp. Soc. Natur. Moscow 3 (1809) 324–344.

[3] S. Das, S. Chakraborty, Analytical solutions for velocity, temperature and concentration distribution in electroosmotic microchannel flows of a non-Newtonian biofluid, Anal. Chim. Acta. 559 (2006) 15.

[4] W.B. Zimmerman, J.M. Rees, T.J. Craven, Rheometry of non-Newtonian electrokinetic flow in a microchannel T-junction, Microfluid. Nanofluid. 2 (2006) 481–492.

[5] C. Zhao, E. Zholkovskij, J.H. Masliyah, C. Yang, Analysis of electroosmotic flow of power-law fluids in a slit microchannel, J. Colloid Interface Sci. 326 (2008) 503–510.

[6] M.L. Olivares, L. Vera-Candioti, C.L.A. Berli, The EOF of polymer solutions, Electrophoresis 30 (2009) 921–929.

[7] C. Zhao, C. Yang, Nonlinear Smoluchowski velocity for electroosmosis of power-law fluids over a surface with arbitrary zeta potentials, Electrophoresis 31 (2010) 973–979.

[8] C. Zhao, C. Yang, Electro-osmotic mobility of non-Newtonian fluids, Biomicrofluidics 5 (2011) 014110.

[9] A. Babaie, A. Sadeghi, M.H. Saidi, Combined electroosmotically and pressure driven flow of power-law fluids in a slit microchannel, J. Non-Newtonian Fluid Mech. 166 (2011) 792–798.

[10] M.A. Vakili, A. Sadeghi, M.H. Saidi, A.A. Mozafari, Electrokinetically driven fluidic transport of power-law fluids in rectangular microchannels, Colloids Surf. A: Physicochem. Eng. Asp. 414 (2012) 440–456.

[11] C.O. Ng, Combined pressure-driven and electroosmotic flow of Casson fluid through a slit microchannel, J. Non-Newtonian Fluid Mech. 198 (2013) 1–9.

[12] C.O. Ng, C. Qi, Electroosmotic flow of a viscoplastic material through a slit channel with walls of arbitrary zeta potential, Phys. Fluids 25 (2013) 103102.

[13] C.O. Ng, C. Qi, Electroosmotic flow of a power-law fluid in a non-uniform microchannel, J. Non-Newtonian Fluid Mech. 208–209 (2014) 118–125.

[14] J. Dhar, U. Ghosh, S. Chakraborty, Alterations in streaming potential in presence of time periodic pressure-driven flow of a power law fluid in narrow confinements with nonelectrostatic ion–ion interactions, Electrophoresis 35 (2014) 662–669.

[15] Q. Zhu, S. Deng, Y. Chen, Periodical pressure-driven electrokinetic flow of power-law fluids through a rectangular microchannel, J. Non-Newtonian Fluid Mech. 203 (2014) 38–50.

[16] C. Qi, C.O. Ng, Electroosmotic flow of a power-law fluid in a slit microchannel with gradually varying channel height and wall potential, Euro. J. Mech. B/Fluids 52 (2015) 160–168.

[17] C. Qi, C.O. Ng, Electroosmotic flow of a power-law fluid through an asymmetrical slit microchannel with gradually varying wall shape and wall potential, Colloids Surf. A: Physicochem. Eng. Asp. 472 (2015) 26–37.

[18] D.C. Duffy, H.L. Gillis, J. Lin, N.F. Sheppard, G.J. Kellogg, Microfabricated centrifugal microfluidic systems: characterization and multiple enzymatic assays, Anal. Chem. 71 (1999) 4669–4678.

[19] M. Madou, J. Zoval, G. Jia, H. Kido, J. Kim, N. Kim, Lab on a CD, Annu. Rev. Biomed. Eng. 8 (2006) 601.

[20] G.J. Wang, W.H. Hsu, Y.Z. Chang, H. Yang, Centrifugal and electric field forces dual-pumping CD-like microfluidic platform for biomedical separation, Biomed. Microdevices 6 (2004) 47–53.

[21] C.C. Chang, C.Y. Wang, Rotating electro-osmotic flow over a plate or between two plates, Phys. Rev. E 84 (2011) 056320.

[22] C.O. Ng, C. Qi, Electro-osmotic flow in a rotating rectangular microchannel, Proc. R. Soc. A 471 (2015) 20150200.

[23] B. Gheshlaghi, H. Nazaripoor, A. Kumar, M. Sadrzadeh, Analytical solution for transient electroosmotic flow in a rotating microchannel, RSC Adv. 6 (2016) 17632.

[24] G.C. Shit, A. Mondal, A. Sinha, P.K. Kundu, Effects of slip velocity on rotating electro-osmotic flow in a slowly varying micro-channel, Colloids Surf. A: Physicochem. Eng. Asp. 489 (2016) 249–255.

[25] Z.Y. Xie, Y.J. Jian, Rotating electroosmotic flow of power-law fluids at high zeta potentials, Colloids Surf. A: Physicochem. Eng. Asp. 461 (2014) 231–239.

[26] S.X. Li, Y.J. Jian, Z.Y. Xie, Q.S. Liu, F.Q. Li, Rotating electro-osmotic flow of third grade fluids between two microparallel plates, Colloids Surf. A: Physicochem. Eng. Asp. 470 (2015) 240–247.

[27] P. Abhimanyu, P. Kaushik, P.K. Mondal, S. Chakraborty, Transiences in rotational electro-hydrodynamics microflows of a viscoelastic fluid under electrical double layer phenomena, J. Non-Newtonian Fluid Mech. 231 (2016) 56–67.

[28] R.L. Whitmore, Rheology of the Circulation, Pergamon, London, 1968.

[29] E.W. Merrill, Rheology of blood, Physiol. Rev. 49 (1969) 863–888.

[30] H. Schmid-Schönbein, R.E. Wells, Rheological properties of human erythrocytes and their influence upon anomalous viscosity of blood, Physiol. Rev. 63 (1971) 147–219.

[31] W.P. Walawender, T.Y. Chen, D.F. Cala, An approximate Casson fluid model for tube flow of blood, Biorheol. 12 (1975) 111.

[32] M. Nakamura, T. Sawada, Numerical study on the flow of a non-Newtonian fluid through an axisymmetric stenosis, ASME J. Biomech. Eng. 110 (1988) 137–143.

[33] Y.C. Fung, Biomechanics: Circulation, Springer, New York, 1996.

[34] J.F. Stoltz, M. Singh, P. Riha, Hemorheology in Practice, IOS Press, 1999.

[35] T.C. Papanastasiou, Flows of materials with yield, J. Rheol. 31 (1987) 385.

[36] M. Bercovier, M. Engelman, A finite-element method for incompressible non-Newtonian flows, J. Comput. Phys. 36 (1980) 313–326.

[37] M. Allouche, I.A. Frigaard, G. Sona, Static wall layers in the displacement of two viscoplastic fluids in a plane channel, J. Fluid Mech. 424 (2000) 243–277.